

Observation of the Smallest Three-Dimensional Neutral Boron Cluster

Cong-Qiao Xu[#], Tiantong Wang[#], Chong Wang, Xin-Ran Dong, Huijun Zheng, Ya Zhao, Li-Li Pan, Jiayue Yang, Weiqing Zhang, Guorong Wu, Hua Xie, Gang Li,* Jun Li,* Ling Jiang,* Xueming Yang, and Lai-Sheng Wang*

Abstract: Despite major progress in the investigation of boron cluster anions, direct experimental study of neutral boron clusters remains a significant challenge because of the difficulty in size selection. Here we report a size-specific study of the neutral B₉ cluster using threshold photoionization with a tunable vacuum ultraviolet free electron laser. The ionization potential of B₉ is measured to be 8.45 ± 0.02 eV and it is found to have a heptagonal bipyramid D_{7h} structure, quite different from the planar molecular wheel of the B₉⁻ anionic cluster. Chemical bonding analyses reveal superior stability of the bipyramidal structure arising from delocalized σ and π bonding interactions within the B₇ ring and between the B₇ ring and the capping atoms. Photoionization of B₉ breaks the single-electron B-B bond of the capping atoms, which undergo off-axis distortion to enhance interactions with the B₇ ring in the singlet ground state of B₉⁺. The single-electron B-B bond of the capping atoms appears to be crucial in stabilizing the D_{7h} structure of B₉. This work opens avenues for direct size-dependent experimental studies of a large variety of neutral boron clusters to explore the stepwise development of network structures.

Boron is an important element and finds applications in many areas, such as materials, catalysis, and energy.^[1] Over the past two decades, boron nanoclusters have been

investigated under well-defined experimental conditions to explore the evolution of structures and bonding as a function of cluster size.^[2] Ionic boron clusters facilitate mass-spectrometry-based size selection and thus have been extensively studied. Earlier experimental studies of boron clusters involved photofragmentation and chemical reactivity of B_n⁺ cations.^[3] Boron cluster cations have been found to undergo a quasi-planar-to-cylindrical structural transition at B₁₆⁺.^[4] Photoelectron spectroscopy (PES) in combination with quantum chemical calculations has shown that boron cluster anions (B_n⁻) possess planar or quasi-planar (2D) structures for n ≤ 42.^[2,5] In this size range, the double-ring tubular-type structure of B₂₀⁻ was found to be isoenergetic to the 2D structure.^[5b] Although the borospherene B₄₀⁻ was a higher energy isomer,^[6] the global minimum (GM) of B₃₉⁻ was found to consist of two degenerate chiral borospherenes.^[7] The discovery of the 2D hexagonal B₃₆⁻ cluster provided the first experimental evidence of the viability of 2D boron nanomaterials (borophene),^[5c] which has become a new class of synthetic 2D materials.^[8]

In contrast to the wealth of experimental work on ionic boron clusters, spectroscopic characterization of neutral boron clusters has been scarce due to the difficulty in size selection. The B₃ cluster was first studied in an argon matrix by infrared spectroscopy.^[9] Its electronic spectroscopy was investigated both in a neon matrix and in the gas phase.^[10] Earlier theoretical studies suggested 2D structures for B_n (n = 4–14),^[11] as well as 3D structures for B₁₂.^[12] Joint PES and theoretical study showed that both anionic and neutral

[*] C.-Q. Xu,[#] X.-R. Dong, J. Li, X. Yang
 Department of Chemistry and Guangdong Provincial Key Laboratory of Catalytic Chemistry, Southern University of Science and Technology, Shenzhen 518055, China
 E-mail: junli@mail.tsinghua.edu.cn

T. Wang,[#] C. Wang, H. Zheng, Y. Zhao, J. Yang, W. Zhang, G. Wu, H. Xie, G. Li, L. Jiang, X. Yang
 State Key Laboratory of Molecular Reaction Dynamics and Dalian Coherent Light Source, Dalian Institute of Chemical Physics, Chinese Academy of Sciences, Dalian 116023, China
 E-mail: gli@dicp.ac.cn
 ljiang@dicp.ac.cn

C. Wang, X. Yang
 Institute of Advanced Science Facilities, Shenzhen 518107, China

C. Wang
 Department of Chemical Physics, University of Science and Technology of China, Hefei 230026, China

L.-L. Pan, J. Li
 Department of Chemistry and Engineering Research Center of Advanced Rare-Earth Materials of Ministry of Education, Tsinghua University, Beijing 100084, China

J. Li
 Fundamental Science Center of Rare Earths, Ganjiang Innovation Academy, Chinese Academy of Science, Ganzhou 341000, China

L. Jiang, X. Yang
 Hefei National Laboratory, Hefei 230088, China

L.-S. Wang
 Department of Chemistry, Brown University, Providence, Rhode Island 02912, United States
 E-mail: laisheng_wang@brown.edu

[[#]] C.Q.X. and T.W. contributed equally to this work.

boron clusters for $n < 20$ are planar.^[2c,e, 5a-k] The only direct experimental study on larger neutral boron clusters was done using infrared + ultraviolet two-color ionization spectroscopy on B_{11} , B_{16} , and B_{17} , which were found to be planar or quasi-planar,^[13] similar to their corresponding anions.^[5d,i, k] Even though a theoretical calculation suggested that the GM of B_{14} has a 3D structure,^[14] it has not been confirmed and the smallest 3D neutral boron cluster is not known experimentally. Here we report the first photoionization efficiency (PIE) spectroscopic study of the B_9 cluster, which is found to feature a heptagonal bipyramid structure with B-B bonding through the center of the B_7 ring between the two capping atoms. The B_9 cluster, the smallest 3D neutral boron cluster found thus far, exhibits D_{7h} symmetry with high stability due to delocalized σ and π bonding.

The experimental PIE spectrum of B_9 was measured by using a vacuum ultraviolet free electron laser (VUV-FEL)-based cluster spectroscopic instrument [see Supporting Information for experimental details].^[15] Neutral boron clusters were generated via laser vaporization of a ^{11}B -enriched target in a pulsed supersonic expansion of helium. The B_9 cluster was photoionized by the VUV-FEL and mass-analyzed in a reflectron time-of-flight mass spectrometer. The VUV-FEL was scanned in the wavelength range of 120–155 nm (8.00–10.33 eV) with steps of 0.3 nm. The PIE spectra were obtained by measuring the B_9^+ ion intensity as a function of the VUV-FEL photon energy, normalized by the VUV-FEL pulse energy.

Figure 1 shows the experimental PIE spectrum of B_9 . Since B_9 was prepared in the cold helium molecular beam (the rotational temperature should be less than 10 K and the vibrational temperature could be higher), the ionization potential of B_9 can be extracted from the onset of the PIE curve. As shown in Figure 1, the rising point of the PIE curve appears at 8.45 ± 0.02 eV, which represents the first ionization potential (IP1) of B_9 . The second onset is discernible at 9.61 ± 0.02 eV, which may correspond to the

opening of a second ionization channel (IP2), i.e., the onset of an electronic excited state of B_9^+ , or other low-lying isomers of B_9 . The error bar of ± 0.02 eV was determined by the scan stepsize of the VUV-FEL wavelength.

To understand the experimental spectral features, we performed GM structure searches for neutral B_9 and cationic B_9^+ by using the constrained basin-hopping algorithm in the TGMIn program^[16] and the evolutionary algorithm (see Supporting Information for theoretical details).^[17] The structures were initially optimized at the PBE/TZ2P level of theory and the low-lying isomers within 2.0 eV were then reoptimized at the PBE0/TZ2P level of theory. The electronic energies of the ten low-lying isomers were refined by single-point calculations at the CCSD(T)/cc-pVTZ level of theory using the PBE0/TZ2P optimized geometries. The five lowest-lying isomers of B_9 (labeled **9A–9E**) and B_9^+ (labeled **9A⁺–9E⁺**) are shown in Figure 2. Other low-lying isomers for B_9 and B_9^+ are illustrated in Figures S1 and S2, respectively.

The GM isomer of B_9 (**9A**, D_{7h} , $^2A_1'$) is found to have a high symmetry heptagonal bipyramid structure with a B–B bond between the two capping atoms (Figure 2), as supported by vibrational frequency calculations (Table S1). It should be noted that a C_s and C_{2v} structure was reported previously for B_9 .^[11b,18] The **9B** isomer with C_{2v} symmetry consists of two out-of-plane B atoms bonded to the edge of a wheel-shaped B_7 motif, which is 9.00 kcal/mol higher in energy than the **9A** GM at the CCSD(T)/cc-pVTZ//PBE0/TZ2P level. The **9C** isomer, lying 15.91 kcal/mol above **9A**, is similar to isomer II of the B_9^- anion.^[5f] The **9D** isomer, lying 16.21 kcal/mol above **9A**, is similar to the GM of B_9^- with a wheel-shaped planar B_8 structure.^[5f] The **9E** isomer can be viewed as a hexagonal bipyramid capped by one B atom.

The GM of the B_9^+ cation (**9A⁺**, Figure 2) has a distorted 3D structure, in which the two capping atoms move off axis. The **9B⁺** isomer, 1.53 kcal/mol above **9A⁺** at the CCSD(T)/cc-pVTZ//PBE0/TZ2P level, is similar to **9E**

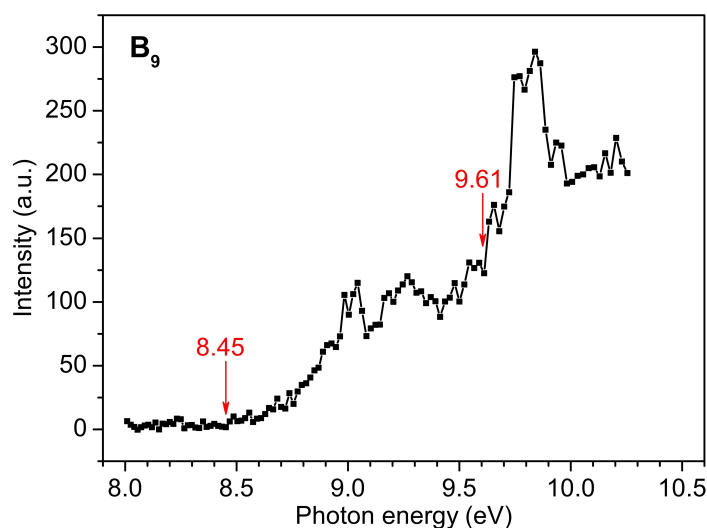


Figure 1. Photoionization efficiency spectrum of B_9 .

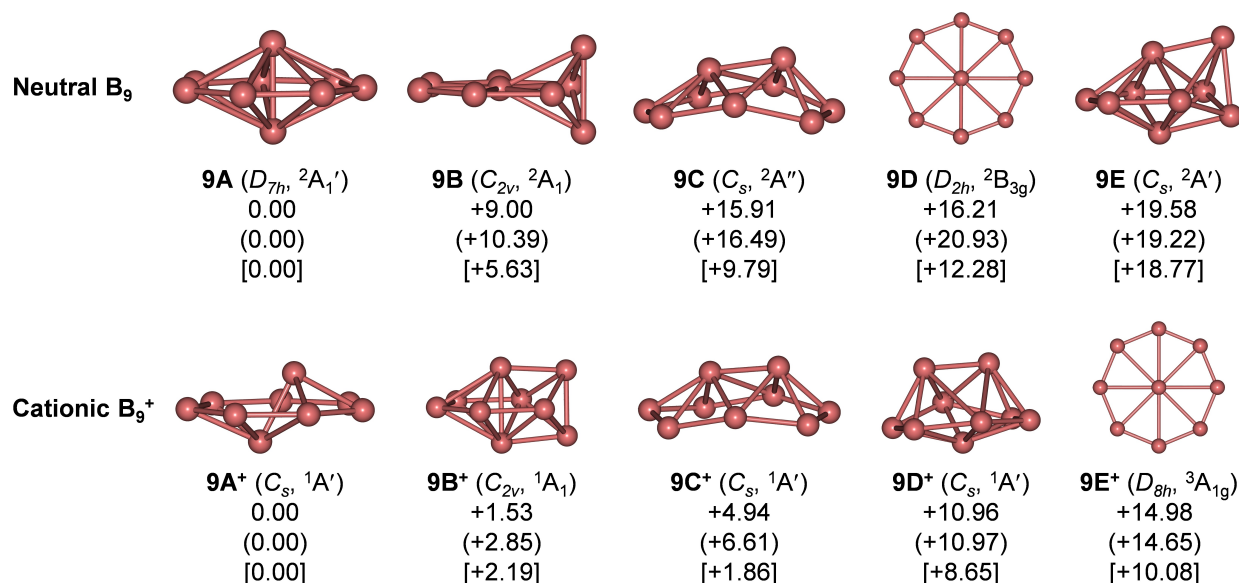


Figure 2. Optimized low-lying structures of neutral B₉ and cationic B₉⁺. The relative energies are given in kcal/mol at the CCSD(T)/cc-pVTZ//PBE0/TZ2P, PBE0/TZ2P (in parentheses), and PBE/TZ2P (in brackets) levels of theory.

of neutral B₉ (Figure 2). Isomer **9C⁺** is similar to isomer **9C** of B₉, whereas isomer **9D⁺** is similar to **9F** of B₉ (Figure S1). The B₉⁺ molecular wheel **9E⁺** is 14.98 kcal/mol higher in energy than the GM of B₉⁺.

The IPs of the B₉ low-lying isomers were calculated to compare with the experimental values. The valence electron configuration of the GM of B₉ (*D*_{7h}, ²A₁[']) is $\dots(2e_1')^2(3a_1')^1$, where the singly occupied molecular orbital (SOMO) 3a₁'

involves B–B bonding between the two capping atoms and the highest occupied molecular orbital (HOMO) 2e₁' involves in-plane σ bonding of the B₇ ring (Figure 3). The IP1 is derived from ionization of the SOMO electron, breaking the B–B bond and resulting in the distorted ground state of B₉⁺ (*C*_s, ¹A₁[']) (Figure S3). The IP2 comes from ionization of an electron from the 2e₁' HOMO, resulting in the slightly distorted excited state of B₉⁺ (*C*_s, ³A₁[']) due to the

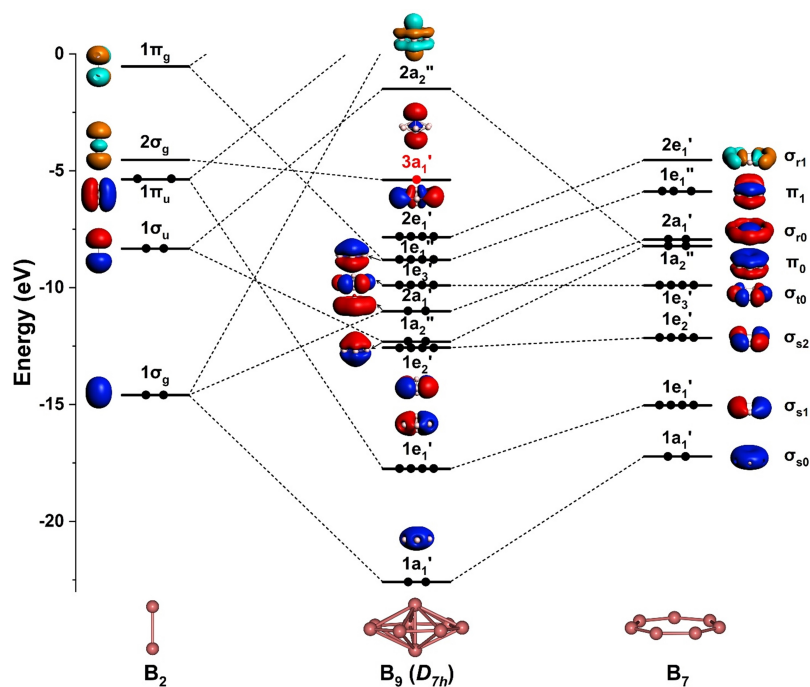


Figure 3. Schematic Kohn–Sham molecular orbital correlation diagram for B₉ (isomer **9A**, *D*_{7h}) at the PBE0/TZ2P level of theory. The non-bonding 1e₃' orbital of B₉ is aligned with the σ_{10} orbital of the B₇ ring for clarity.

Jahn–Teller effect (Figure S4). The IP1 and IP2 of **9A** are calculated to be 8.31 and 9.59 eV at the CCSD(T)/cc-pVTZ//PBE0/TZ2P level (Table 1, Figure S4), respectively, in excellent agreement with the experimental values of 8.45 ± 0.02 and 9.61 ± 0.02 eV. The calculated IP1 and IP2 values of isomers **9B–9E** are much lower than the experimental values (Table S2), indicating these isomers can be ruled out. The excellent agreement between the experimental and theoretical IPs provides considerable credence to the **9A** GM for B_9 .

The structure and bonding of the B_9 GM are interesting. The B–B bond lengths in the B_7 ring and between the two axial capping atoms are calculated to be 1.53 Å and 1.70 Å at the PBE0/TZ2P level of theory, respectively (Table S3). The B–B single-bond length is 1.70 Å, according to Pyykkö's atomic covalent radii.^[19] Thus, there are multiple B–B bond characters around the B_7 ring and significant covalent bonding between the axial B atoms, whereas there is only weak bonding between the capping atoms and the B_7 ring. Atomic charge and spin density analyses indicate that there is a slight charge transfer from the axial atoms to the B_7 ring (Table S4). Removal of the SOMO $3a_1'$ electron breaks the axial B–B bond in B_9^+ , resulting in significant off-axis distortion of the capping atoms to enhance their interactions with the B_7 ring at the expense of the B–B bonding in the B_7 ring, which is weakened (Table S5). The resulted GM **9A**⁺ exhibits C_s symmetry with a closed-shell electron configuration ($^1A'$), whereas the D_{7h} structure is a saddle point on the potential energy surface (Figure S5). Figure S5 also shows that the triplet excited state of B_9^+ is a slightly distorted pseudo- D_{7h} structure, where the distortion only occurs in the B_7 ring because the HOMO electron removed only involves σ bonding in the B_7 ring (Figure 3). The large geometry change between the ground state of B_9^+ and that of B_9 is consistent with the low intensity near threshold for the first ionization channel; the minor structural change between the triplet excited state of B_9^+ relative to neutral B_9 underlies the sharp rise of ionization cross section for the second ionization channel (Figure 1).

The stability and structural change between B_9 and B_9^+ can be rationalized in more detail via orbital interactions. The Kohn–Sham MO correlation diagram between the B–B and B_7 fragments and the canonical molecular orbitals (CMOs) of B_9 and B_9^+ is given in Figure S3. The B_9 cluster has a valence electron configuration of $\dots(2e_1')^4(3a_1')^1(2a_2'')^0$. The SOMO represents σ bonding between the s - p hybridized orbitals of the two capping atoms, consistent with the predominant spin density populations (Figure S6 and Table S4). In addition to the $3a_1'$ orbital, there are two types of

MOs, one responsible for the bonding within the B_7 ring and the other for the weak bonding between the two axial atoms and the B_7 ring. According to the localized coordinate system (Figure S7), the 28 $2s$ – $2p$ valence atomic orbitals (AOs) on the B_7 ring are classified into four types: σ_s , $\sigma(t)_p$, $\sigma(r)_p$, and π_p , where t and r represents tangential and radial bonding, respectively. The occupied $\sigma(t)_p$ orbitals (σ_{t0}) and σ_s orbitals are mainly responsible for bonding within the B_7 ring while the occupied π_p orbitals (π_0 , π_1) and $\sigma(r)_p$ orbital (σ_{r0}) for bonding between the axial B–B atoms and the B_7 ring, reminiscent of bonding features in the inverse sandwich complexes, $Ln_2B_n^-$ ($Ln = La, Pr; n = 7-9$).^[20] Slightly different from $Ln_2B_n^-$, the occupied σ_{s0} and σ_{s1} orbitals in B_9 contribute to bonding between the B–B and the B_7 ring only as a result of symmetry compatibility with the $2s$ – $2p$ valence orbitals of the axial B atoms.

Principal interacting orbital (PIO) analyses were carried out to quantitatively evaluate the orbital interactions between the capping atoms and the B_7 ring for B_9 ; four major orbital interactions were found, as shown in Figure S8. The two dominant interactions arise from the π bonding between the B_2 $1\pi_g$ and B_7 π_1 orbitals and the σ bonding between the B_2 $1\pi_u$ and B_7 σ_{s1} orbitals, contributing 32.3% and 30.7% to the total interactions, respectively. Compared to the $5d$ AOs of lanthanide in $Ln_2B_n^-$, the lower-lying $2s$ and $2p$ AOs of the capping B atoms in B_9 enable more efficient overlaps with the B_7 ring, leading to the third interaction that signifies σ bonding between the B_2 $1\sigma_g$ orbital and both the σ_{s0} and σ_{r0} orbitals of B_7 , which accounts for 17.6% contribution to the total interactions. The fourth interaction features $1\sigma_u(B_2)$ – $\pi_0(B_7)$ bonding, with a contribution of 17.3%. Overall, three σ bonding and three π bonding are identified, consistent with the CMO picture. Energy decomposition analysis combined with natural orbital of chemical valence (EDA–NOCV) analyses yield four similar major orbital terms (Table S6), except for the overestimation of the $1\pi_u(B_2)$ – $\sigma_{s1}(B_7)$ interaction due to the assignment of B_2^+ ($1\pi_u^4 2\sigma_g^1$) and B_7^- ($\dots\pi_1^4$) fragments. Especially noteworthy is that the interaction between the singly occupied B–B σ orbital and the B_7 ring only contributes 0.29% to the total interactions, indicative of a negligible role. As shown in Table S6, the stabilization energy of B_9 mainly arises from the orbital interaction, in comparison to the electrostatic interaction.

The bonding in B_9 is further analyzed by the adaptive natural density partitioning (AdNDP) approach (Figure 4), which reveals seven localized two-center two-electron (2c–2e) B–B σ bonds in the B_7 ring and one 2c–1e B–B σ bond between the capping atoms. The interactions between the capping atoms and the B_7 ring are responsible for the extensively delocalized bonds, which include three 9c–2e σ bonds arising from the interactions between $1\sigma_g/1\pi_u$ orbitals of B_2 and $\sigma_s/\sigma(r)_p$ orbitals of B_7 and three 9c–2e π bonds arising from the interactions between $1\sigma_u/1\pi_g$ orbitals of B_2 and π_p orbitals of B_7 . These delocalized bonds further strengthen the B–B bonds in the B_7 ring, resulting in their multiple bond characters. Both the delocalized σ and π bonds satisfy the $4n+2$ Hückel rule, suggesting double

Table 1: Comparison of experimental ionization potentials (IP, in eV) with theoretical values of the global-minimum structure **9A** calculated at the CCSD(T)/cc-pVTZ//PBE0/TZ2P, PBE0/TZ2P, and PBE/TZ2P levels of theory.

IP	Expt.	CCSD(T)	PBE0	PBE
IP1	8.45 ± 0.02	8.31	8.44	8.37
IP2	9.61 ± 0.02	9.59	9.49	9.41

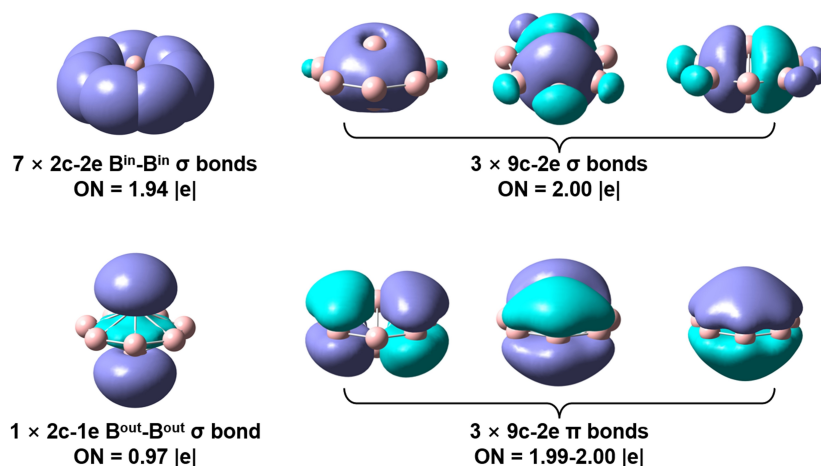


Figure 4. The AdNDP bonding analysis for the GM of B₉ (D_{7h} , $^2A_1'$) at the PBE0/cc-pVTZ level. ON stands for occupation number. Bⁱⁿ stands for the boron atoms in the B₇ plane and B^{out} for the capping atoms.

aromaticity that underlies the high stability of the B₉ GM, in analogy to that of La₂B₇⁻.^[20b]

To address the origin of structural change from B₉ to B₉⁺, we also analyzed the chemical bonding in B₉⁺. It can be seen from the MO correlation diagram (Figure S3) and CMO (Figure S9) that upon photoionization, the electron in the SOMO of B₉ is removed, breaking the B-B σ bond between the capping atoms in B₉⁺. Consequently, the capping atoms distort off axis towards the B₇ ring. As further revealed by the AdNDP analysis of B₉⁺ (Figure S10), similar localized B-B σ bond in the B₇ ring and delocalized σ and π bonds are identified as compared to neutral B₉, with the absence of the 2c-1e B-B σ bond between the capping atoms. Interestingly, in the triplet excited state of B₉⁺ (C_s , $^3A'$), the 2c-1e B-B bond between the capping atoms is intact, underlying its pseudo- D_{7h} structure, where the slight distortion occurs in the B₇ ring.

It is interesting to compare the GM of the B₉ neutral with that of the B₉⁻ anion, which is a perfect B@B₈⁻ molecular wheel with D_{8h} symmetry and double aromaticity.^[5c,f] The D_{7h} structure of B₉⁻ is a transition state with two imaginary frequencies, for which geometry optimizations along the imaginary coordinates lead to a low-lying isomer with a distorted heptagonal bipyramid C_s structure due to a second-order Jahn–Teller effect.^[5f] This C_s structure of B₉⁻ has a two-electron B-B bond between the two capping atoms, which is much higher in energy above the D_{8h} global minimum in the density functional theory calculations but is much closer in energy to the D_{8h} global minimum from the most accurate wave-function theory ab initio methods, as reported previously.^[5f] B₉⁻ is a key member of the borozene family,^[21] consisting additionally of B₇³⁻ (B@B₆³⁻) and B₈²⁻ (B@B₇²⁻), which all have similar double aromaticity. The B₆ ring in B₇³⁻ is too small so that the central B atom is squeezed out of plane slightly to give it a bowl shape with C_{6v} symmetry, whereas the B₇ ring in B₈²⁻ is perfect, making it the most stable borozene. The B₈ ring in B₉⁻ is slightly too large to host the central B atom, which is the main reason why a low-lying and low-symmetry isomer

becomes competitive to co-exist with the B₉⁻ wheel GM experimentally.^[5c,f] The HOMO of B₉⁻ is the degenerate π MO. Thus, removing an electron from B₉⁻ weakens the π aromaticity, so that the Jahn–Teller distorted B₉ wheel becomes the fourth isomer on the neutral potential energy surface, 16.21 kcal/mol higher in energy than the D_{7h} GM (Figure 2). On the other hand, double aromaticity is restored in the D_{7h} B₉ GM (Figure 4). Thus, double aromaticity can be viewed as the driving force for the different GM structures of B₉⁻ and B₉.

In summary, the size-specific photoionization efficiency spectrum of B₉ was measured by using a tunable vacuum ultraviolet free electron laser and analyzed with the aid of quantum chemical calculations. B₉ was characterized to be the smallest 3D neutral boron cluster, which features a heptagonal bipyramid structure with B-B bonding between the capping atoms. Chemical bonding analyses reveal delocalized σ and π bonding interactions in B₉, which give rise to double aromaticity and account for the superior stability of its D_{7h} GM. Upon VUV photoionization, the single-electron B-B σ bond between the capping atoms is broken in the ground state of B₉⁺, resulting in off-axis distortions of the capping atoms to enhance interactions with the B₇ ring. The second ionization channel of B₉ reaches the triplet excited state of B₉⁺, which maintains a pseudo- D_{7h} structure because of the axial single-electron B-B bond. The observation of the smallest 3D neutral boron cluster and comparison of its stability with the B₉⁻ anionic cluster advances our understanding of bonding in boron clusters. The initial experimental result on B₉ suggests that the VUV-FEL facility is promising to allow direct spectroscopic studies of neutral clusters in a size-selected fashion.

Supporting Information

Experimental and theoretical methods, Figures S1–S10, Tables S1–S6, and references (PDF).

Acknowledgements

The authors gratefully acknowledge the staff members of the Dalian Coherent Light Source (31127.02.DCLS) for technical support and assistance in data collection. This work was supported by the National Natural Science Foundation of China (NSFC) (22125303, 22033005, 92361302, 92061203, 22103082, 22273101, 22288201, and 21327901), the US National Science Foundation (CHE-2403841 to L.S.W.), NSFC Center for Single-Atom Catalysis (22388102), the National Key Research and Development Program of China (2021YFA1400501), the Strategic Priority Research Program of the Chinese Academy of Sciences (XDB0970100), the Innovation Program for Quantum Science and Technology (2021ZD0303304), the Scientific Instrument Developing Project of the Chinese Academy of Sciences (GJJSTD20220001), the International Partnership Program of the Chinese Academy of Sciences (121421KYSB20170012), Shenzhen Science and Technology Program (RCYX20231211090357078), Dalian Institute of Chemical Physics (DICP DCLS201702), the startup fund for the Fundamental Science Center of Rare Earths, Ganjiang Innovation Academy, Chinese Academy of Sciences, and Guangdong Provincial Key Laboratory of Catalysis (2020B121201002). Computational resources were supported by the Center for Computational Science and Engineering at Southern University of Science and Technology, CHEM high-performance supercomputer cluster (CHEM-HPC), and Tsinghua National Laboratory for Information Science and Technology.

Conflict of Interest

The authors declare no conflict of interest.

Data Availability Statement

The data that support the findings of this study are available from the corresponding author upon reasonable request.

Keywords: boron clusters · structures and bonding · photoionization · vacuum ultraviolet free electron laser · quantum chemical calculations

- [1] a) J. T. Grant, C. A. Carrero, F. Goeltl, J. Venegas, P. Mueller, S. P. Burt, S. E. Specht, W. P. McDermott, A. Chierigato, I. Hermans, *Science* **2016**, *354*, 1570–1573; b) M.-A. Legare, C. Prancevicus, H. Braunschweig, *Chem. Rev.* **2019**, *119*, 8231–8261; c) H. Tang, Y. Wang, X. Ni, K. Watanabe, T. Taniguchi, P. Jarillo-Herrero, S. Fan, E. Mazur, A. Yacoby, Y. Cao, *Nature* **2024**, *632*, 1038–1044.
- [2] a) A. N. Alexandrova, A. I. Boldyrev, H. J. Zhai, L. S. Wang, *Coord. Chem. Rev.* **2006**, *250*, 2811–2866; b) L. S. Wang, *Int. Rev. Phys. Chem.* **2016**, *35*, 69–142; c) W. L. Li, X. Chen, T. Jian, T. T. Chen, J. Li, L. S. Wang, *Nat. Chem. Rev.* **2017**, *1*, 0071; d) W. L. Li, H. S. Hu, Y. F. Zhao, X. Chen, T. T. Chen, T. Jian, L. S. Wang, J. Li, *Sci. Sin.: Chim.* **2018**, *48*, 98–107; e) T. Jian, X. N. Chen, S. D. Li, A. I. Boldyrev, J. Li, L. S. Wang, *Chem. Soc. Rev.* **2019**, *48*, 3550–3591.
- [3] a) L. Hanley, S. L. Anderson, *J. Phys. Chem.* **1987**, *91*, 5161–5163; b) L. Hanley, S. L. Anderson, *J. Chem. Phys.* **1988**, *89*, 2848–2860; c) L. Hanley, J. L. Whitten, S. L. Anderson, *J. Phys. Chem.* **1988**, *92*, 5803–5812; d) P. A. Hintz, M. B. Sowa, S. A. Ruatta, S. L. Anderson, *J. Chem. Phys.* **1991**, *94*, 6446–6458.
- [4] a) E. Oger, N. R. M. Crawford, R. Kelting, P. Weis, M. M. Kappes, R. Ahlrichs, *Angew. Chem. Int. Ed.* **2007**, *46*, 8503–8506; b) M. R. Fagiani, X. Song, P. Petkov, S. Debnath, S. Gewinner, W. Schoellkopf, T. Heine, A. Fielicke, K. R. Asmis, *Angew. Chem. Int. Ed.* **2017**, *56*, 501–504.
- [5] a) H. J. Zhai, L. S. Wang, A. N. Alexandrova, A. I. Boldyrev, *J. Chem. Phys.* **2002**, *117*, 7917–7924; b) A. N. Alexandrova, A. I. Boldyrev, H. J. Zhai, L. S. Wang, E. Steiner, P. W. Fowler, *J. Phys. Chem. A* **2003**, *107*, 1359–1369; c) H. J. Zhai, L. S. Wang, A. N. Alexandrova, A. I. Boldyrev, *J. Phys. Chem. A* **2003**, *107*, 9319–9328; d) H. J. Zhai, B. Kiran, J. Li, L. S. Wang, *Nat. Mater.* **2003**, *2*, 827–833; e) H. J. Zhai, A. N. Alexandrova, K. A. Birch, A. I. Boldyrev, L. S. Wang, *Angew. Chem. Int. Ed.* **2003**, *42*, 6004–6008; f) L. L. Pan, J. Li, L. S. Wang, *J. Chem. Phys.* **2008**, *129*, 024302; g) A. N. Alexandrova, A. I. Boldyrev, H. J. Zhai, L. S. Wang, *J. Phys. Chem. A* **2004**, *108*, 3509–3517; h) B. Kiran, S. Bulusu, H. J. Zhai, S. Yoo, X. C. Zeng, L. S. Wang, *Proc. Natl. Acad. Sci. USA* **2005**, *102*, 961–964; i) A. P. Sergeeva, D. Y. Zubarev, H. J. Zhai, A. I. Boldyrev, L. S. Wang, *J. Am. Chem. Soc.* **2008**, *130*, 7244–7246; j) W. Huang, A. P. Sergeeva, H. J. Zhai, B. B. Averkiev, L. S. Wang, A. I. Boldyrev, *Nat. Chem.* **2010**, *2*, 202–206; k) A. P. Sergeeva, B. B. Averkiev, H. J. Zhai, A. I. Boldyrev, L. S. Wang, *J. Chem. Phys.* **2011**, *134*, 224304; l) Z. A. Piazza, W. L. Li, C. Romanescu, A. P. Sergeeva, L. S. Wang, A. I. Boldyrev, *J. Chem. Phys.* **2012**, *136*, 104310; m) A. P. Sergeeva, Z. A. Piazza, C. Romanescu, W. L. Li, A. I. Boldyrev, L. S. Wang, *J. Am. Chem. Soc.* **2012**, *134*, 18065–18073; n) I. A. Popov, Z. A. Piazza, W. L. Li, L. S. Wang, A. I. Boldyrev, *J. Chem. Phys.* **2013**, *139*, 144307; o) Z. A. Piazza, H. S. Hu, W. L. Li, Y. F. Zhao, J. Li, L. S. Wang, *Nat. Commun.* **2014**, *5*, 3113; p) W. L. Li, Y. F. Zhao, H. S. Hu, J. Li, L. S. Wang, *Angew. Chem. Int. Ed.* **2014**, *53*, 5540–5545; q) Z. A. Piazza, I. A. Popov, W. L. Li, R. Pal, X. C. Zeng, A. I. Boldyrev, L. S. Wang, *J. Chem. Phys.* **2014**, *141*, 034303; r) W. L. Li, Q. Chen, W. J. Tian, H. Bai, Y. F. Zhao, H. S. Hu, J. Li, H. J. Zhai, S. D. Li, L. S. Wang, *J. Am. Chem. Soc.* **2014**, *136*, 12257–12260; s) W. L. Li, R. Pal, Z. A. Piazza, X. C. Zeng, L. S. Wang, *J. Chem. Phys.* **2015**, *142*, 204305; t) Y. J. Wang, Y. F. Zhao, W. L. Li, T. Jian, Q. Chen, X. R. You, T. Ou, X. Y. Zhao, H. J. Zhai, S. D. Li, J. Li, L. S. Wang, *J. Chem. Phys.* **2016**, *144*, 064307; u) H. R. Li, T. Jian, W. L. Li, C. Q. Miao, Y. J. Wang, Q. Chen, X. M. Luo, K. Wang, H. J. Zhai, S. D. Li, L. S. Wang, *Phys. Chem. Chem. Phys.* **2016**, *18*, 29147–29155; v) Q. Chen, W. J. Tian, L. Y. Feng, H. G. Lu, Y. W. Mu, H. J. Zhai, S. D. Li, L. S. Wang, *Nanoscale* **2017**, *9*, 4550–4557; w) J. Czekner, L. F. Cheung, L. S. Wang, *J. Phys. Chem. C* **2017**, *121*, 10752–10759; x) X. M. Luo, T. Jian, L. J. Cheng, W. L. Li, Q. Chen, R. Li, H. J. Zhai, S.-D. Li, A. I. Boldyrev, J. Li, L. S. Wang, *Chem. Phys. Lett.* **2017**, *683*, 336–341; y) Q. Chen, W. L. Li, X. Y. Zhao, H. R. Li, L. Y. Feng, H. J. Zhai, S. D. Li, L. S. Wang, *Eur. J. Inorg. Chem.* **2017**, 4546–4551; z) A. P. Sergeeva, I. A. Popov, Z. A. Piazza, W. L. Li, C. Romanescu, L. S. Wang, A. I. Boldyrev, *Acc. Chem. Res.* **2014**, *47*, 1349–1358; aa) Q. Chen, T. T. Chen, H. R. Li, X. Y. Zhao, W. J. Chen, H. J. Zhai, S. D. Li, L. S. Wang, *Nanoscale* **2019**, *11*, 9698–9704; ab) H. Bai, T. T. Chen, Q. Chen, X. Y. Zhao, Y. Y. Zhang, W. J. Chen, W. L. Li, L. F. Cheung, B. Bai, J. Cavanagh, W. Huang, S. D. Li, J. Li, L. S. Wang, *Nanoscale* **2019**, *11*, 23286–23295.

- [6] H. J. Zhai, Y. F. Zhao, W. L. Li, Q. Chen, H. Bai, H. S. Hu, Z. A. Piazza, W. J. Tian, H. G. Lu, Y. B. Wu, Y. W. Mu, G. F. Wei, Z. P. Liu, J. Li, S. D. Li, L. S. Wang, *Nat. Chem.* **2014**, *6*, 727–731.
- [7] Q. Chen, W. L. Li, Y. F. Zhao, S. Y. Zhang, H. S. Hu, H. Bai, H. R. Li, W. J. Tian, H. G. Lu, H. J. Zhai, S. D. Li, J. Li, L. S. Wang, *ACS Nano* **2015**, *9*, 754–760.
- [8] a) A. J. Mannix, X.-F. Zhou, B. Kiraly, J. D. Wood, D. Alducin, B. D. Myers, X. Liu, B. L. Fisher, U. Santiago, J. R. Guest, M. J. Yacaman, A. Ponce, A. R. Oganov, M. C. Hersam, N. P. Guisinger, *Science* **2015**, *350*, 1513–1516; b) B. Feng, J. Zhang, Q. Zhong, W. Li, S. Li, H. Li, P. Cheng, S. Meng, L. Chen, K. Wu, *Nat. Chem.* **2016**, *8*, 564–569.
- [9] S. Li, R. J. VanZee, W. Weltner, *Chem. Phys. Lett.* **1996**, *262*, 298–302.
- [10] a) P. Cias, M. Araki, A. Denisov, J. P. Maier, *J. Chem. Phys.* **2004**, *121*, 6776–6778; b) A. Batalov, J. Fulara, I. Shnitko, J. P. Maier, *Chem. Phys. Lett.* **2005**, *404*, 315–317; c) L. Chacaga, E. B. Jochnowitz, Z. Guennoun, H. Ding, J. P. Maier, *Int. J. Mass Spectrom.* **2009**, *280*, 174–178.
- [11] a) I. Boustani, *Chem. Phys. Lett.* **1995**, *240*, 135–140; b) I. Boustani, *Phys. Rev. B* **1997**, *55*, 16426–16438.
- [12] R. Kawai, J. H. Weare, *J. Chem. Phys.* **1991**, *95*, 1151–1159.
- [13] C. Romanescu, D. J. Harding, A. Fielicke, L. S. Wang, *J. Chem. Phys.* **2012**, *137*, 014317.
- [14] L. Cheng, *J. Chem. Phys.* **2012**, *136*, 104301.
- [15] G. Li, C. Wang, Q. Li, H. Zheng, T. Wang, Y. Yu, M. Su, D. Yang, L. Shi, J. Y. Yang, Z. G. He, H. Xie, H. J. Fan, W. Q. Zhang, D. X. Dai, G. R. Wu, X. M. Yang, L. Jiang, *Rev. Sci. Instrum.* **2020**, *91*, 034103.
- [16] a) Y. F. Zhao, X. Chen, J. Li, *Nano Res.* **2017**, *10*, 3407–3420; b) X. Chen, Y. F. Zhao, L. S. Wang, J. Li, *Comput. Theor. Chem.* **2017**, *1107*, 57–65; c) X. Chen, Y. F. Zhao, Y. Y. Zhang, J. Li, *J. Comput. Chem.* **2019**, *40*, 1105–1112.
- [17] a) A. R. Oganov, C. W. Glass, *J. Chem. Phys.* **2006**, *124*, 244704; b) A. R. Oganov, A. O. Lyakhov, M. Valle, *Acc. Chem. Res.* **2011**, *44*, 227–237; c) A. O. Lyakhov, A. R. Oganov, H. T. Stokes, Q. Zhu, *Comput. Phys. Commun.* **2013**, *184*, 1172–1182.
- [18] T. B. Tai, D. J. Grant, M. T. Nguyen, D. A. Dixon, *J. Phys. Chem. A* **2010**, *114*, 994–1007.
- [19] P. Pyykkö, M. Atsumi, *Chem.-Eur. J.* **2009**, *15*, 186–197.
- [20] a) W. L. Li, T. T. Chen, D. H. Xing, X. Chen, J. Li, L. S. Wang, *Proc. Natl. Acad. Sci. USA* **2018**, *115*, E6972–E6977; b) T. T. Chen, W. L. Li, J. Li, L. S. Wang, *Chem. Sci.* **2019**, *10*, 2534–2542.
- [21] a) W. L. Li, T. T. Chen, W. J. Chen, J. Li, L. S. Wang, *Nat. Commun.* **2021**, *12*, 6467; b) W. J. Tian, W. J. Chen, M. Yan, R. Li, Z. H. Wei, T. T. Chen, Q. Chen, H. J. Zhai, S. D. Li, L. S. Wang, *Chem. Sci.* **2021**, *12*, 8157–8164; c) W.-J. Chen, A. S. Pozdeev, H. W. Choi, A. I. Boldyrev, D. F. Yuan, I. A. Popov, L. S. Wang, *Phys. Chem. Chem. Phys.* **2024**, *26*, 12928–12938; d) L. S. Wang, *Acc. Chem. Res.* **2024**, *57*, 2428–2436.

Manuscript received: October 3, 2024

Accepted manuscript online: January 14, 2025

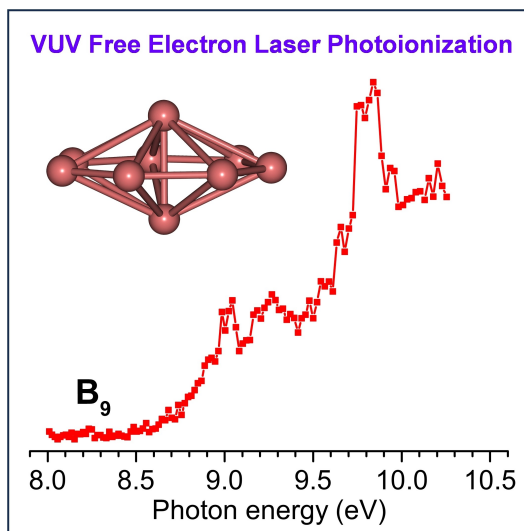
Version of record online: ■■■, ■■■

Communication

Main-Group Chemistry

C.-Q. Xu, T. Wang, C. Wang, X.-R. Dong,
H. Zheng, Y. Zhao, L.-L. Pan, J. Yang,
W. Zhang, G. Wu, H. Xie, G. Li,* J. Li,*
L. Jiang,* X. Yang, L.-
S. Wang* e202419089

Observation of the Smallest Three-Dimensional Neutral Boron Cluster



The photoionization efficiency spectrum of B₉ was measured by using VUV free electron laser. B₉ was characterized to be the smallest 3D neutral boron cluster with a heptagonal bipyramid *D*_{7h} struc-

ture, quite different from the planar molecular wheel of B₉. A single-electron B-B bond between the capping atoms is found to be crucial in stabilizing the *D*_{7h} structure of B₉.